Results in Physics 8 (2018) 671–682

Contents lists available at ScienceDirect

Results in Physics

journal homepage: www.journals.elsevier.com/results-in-physics

# Computational modeling of unsteady third-grade fluid flow over a vertical cylinder: A study of heat transfer visualization

G. Janardhana Reddy *, Ashwini Hiremath, Mahesh Kumar

*Department of Mathematics, Central University of Karnataka, Kalaburagi, India*

ARTICLE INFO

*Article history:*
Received 19 October 2017
Received in revised form 1 December 2017
Accepted 18 December 2017
Available online 23 December 2017

*Keywords:*
Third-grade fluid
Heat function
Boussinesq's approximation
Vertical cylinder
Implicit method
Prandtl number

ABSTRACT

The present paper aims to investigate the effect of Prandtl number for unsteady third-grade fluid flow over a uniformly heated vertical cylinder using Bejan's heat function concept. The mathematical model of this problem is given by highly time-dependent non-linear coupled equations and are resolved by an efficient unconditionally stable implicit scheme. The time histories of average values of momentum and heat transport coefficients as well as the steady-state flow variables are displayed graphically for distinct values of non-dimensional control parameters arising in the system. As the non-dimensional parameter value gets amplified, the time taken for the fluid flow variables to attain the time-independent state is decreasing. The dimensionless heat function values are closely associated with an overall rate of heat transfer. Thermal energy transfer visualization implies that the heat function contours are compact in the neighborhood of the leading edge of the hot cylindrical wall. It is noticed that the deviations of flow-field variables from the hot wall for a non-Newtonian third-grade fluid flow are significant compared to the usual Newtonian fluid flow.



## Introduction

During the past decades, the concept of boundary layer flow with heat transfer has gained considerable attention due to its vital role in industry and manufacturing processes. In particular, the free convective flow past a cylinder has a broad range of applications, such as heat exchanger, filtration screens used for clarifying suspensions, membrane-based separation modules, hot rolling, food product and polymer fiber spinning, etc.

Also, the study of the rate of heat transfer is significant since the cooling rate has a wide impact on the quality of the output and it has many industrial, chemical, residential and commercial applications. The non-Newtonian fluids with heat transfer have gained great importance in science and technology applications. These fluids demarcated by a non-linear constitutive correlation between the strain and the stress. Various mathematical models have existed and explained the behavior of non-Newtonian relationship from that of the Newtonian fluids. The non-Newtonian fluid flow has acquired particular attention because of their rich scientific applications which include the manufacture of synthetic fluids, electrorheological fluids, movement of biological fluids, manufacture of plastic products by injection and extrusion, the production of paints, chemicals in district heating and cooling systems, etc. Numerous studies [1–4] were carried out upon non-Newtonian fluids with several flow formations. Rani and Reddy [5] examined the time-dependent free convection flow of the non-Newtonian fluid past a cylinder with Dufour and Soret effects. Recently, Odelu et al. [6] studied the mixed convection flow of non-Newtonian Jeffrey fluid between two parallel plates. Also, Pop [7] analyzed the non-Newtonian Casson fluid in a cavity with radiation and viscous dissipation effects. Furthermore, Umavathi and Sheremet [8] examined the flow of non-Newtonian micropolar fluid in a porous medium using stability analysis.

In general, there are many non-Newtonian fluid theories are available in the literature because of its versatile applications in medical technology and industry. Out of those, viscoelastic fluids gained a unique reputation from the scholars in the research field. Rivlin and Ericksen [9] have classified the viscoelastic fluids. Truesdell and Noll [10] have introduced constitutive equations for the stress tensor. Depending upon their rheological properties, these fluids are sorted into many subclasses. A deliberation on various types of these fluid models can be found in [11–17]. Amongst these fluids of a differential type model of n-grade, the simplest subclass is the second-grade fluid model. It can predict the normal stress differences which are the characteristics of non-Newtonian fluids

* Corresponding author.
*E-mail address:* gjr@cuk.ac.in (G.J. Reddy).

https://doi.org/10.1016/j.rinp.2017.12.054
2211-3797/

**Nomenclature**

| | |
|---|---|
| $C_p$ | specific heat at constant pressure |
| $\overline{C_f}$ | dimensionless average momentum transport coefficient |
| $g'$ | acceleration due to gravity |
| $Gr$ | Grashof number |
| $k$ | thermal conductivity |
| $\overline{Nu}$ | average heat transport coefficient |
| $Pr$ | Prandtl number |
| $r_o$ | radius of the cylinder |
| $t'$ | time |
| $t$ | dimensionless time |
| $P$ | fluid pressure |
| $I$ | identity tensor |
| $T'$ | temperature |
| $T$ | dimensionless temperature |
| $T^*$ | matrix transposition |
| $S_1, S_2, S_3$ | Rivlin and Ericksen tensors |
| $tr$ | trace |
| $\frac{d}{dt}$ | material time derivative |
| $x$ | axial coordinate |
| $r$ | radial coordinate |
| $u$, $v$ | velocity components in ($x$, $r$) coordinate system |
| $X$ | dimensionless axial coordinate |
| $R$ | dimensionless radial coordinate |
| $U$, $V$ | dimensionless velocity components in ($X$, $R$) directions, respectively |

*Greek letters*

| | |
|---|---|
| $\alpha_1, \alpha_2$ | second-grade fluid parameters |
| $\alpha_1^*, \alpha_2^*, \beta_1^*, \beta_2^*, \beta_3^*$ | rheological material moduli |
| $\beta$ | third-grade fluid parameter |
| $\tau$ | Cauchy stress tensor |
| $\alpha$ | thermal diffusivity |
| $\beta_T$ | volumetric coefficient of thermal expansion |
| $\rho$ | density |
| $\mu$ | viscosity of the fluid |
| $\vartheta$ | kinematic viscosity |
| $\psi$ | stream function |
| $\Omega$ | dimensionless heat function |
| $\Omega'$ | heat function |

*Subscripts*

| | |
|---|---|
| $w$ | wall conditions |
| $f$, $g$ | grid levels in ($X$, $R$) coordinate system |
| $\infty$ | ambient conditions |

*Superscript*

| | |
|---|---|
| $h$ | time level |

and does not take into account the shear thickening and shear thinning phenomenon. But the third-grade fluid model is capable of predicting normal stress differences and shear thickening/shear thinning phenomenon. The third-grade fluid model has been extensively used owing to its rich mathematical background compared with other polar fluid models. The fluids such as slurry flows, dilute polymer solutions (e.g., polyisobutylene, methylmethacrylate in n butyl acetate, polyethylene oxide in water, etc.), molten plastics (e.g., contraband items, plastic keys), food rheology polymers mixed with Newtonian solvents, manufacturing oils and polymer melts like high-viscosity silicone oils are some of the examples of these third-grade fluids. Analytical treatment has been done on the third-grade fluid model [18–21]. Hayat et al. [22] investigated the unsteady flow behavior of a third-grade fluid with Soret and Dufour effects using similarity transformation techniques. Hayat et al. [23] showed that the velocity profile is higher for third-grade fluid in comparison with Newtonian and second-grade fluids for different geometries. Furthermore, few researchers studied the third-grade fluid model with an entropy concept in a channel flow [24,25]. Recently, Hayat et al. [26] studied the heat transfer analysis for third-grade fluid in the presence of Joules heating, viscous dissipation, and thermal radiation effects. Third-grade fluid flow model due to a linearly stretching sheet is demonstrated by Imtiaz et al. [27]. Also, Samuel et al. [28] analyzed the reactive third-grade fluid flow with irreversibility concept.

Conventionally thermal convection fluid dynamics research problems are analyzed only with the aid of streamlines and isotherms. In a given domain isotherms will furnish information on the temperature distribution. However, using them to visualize the direction and heat transfer intensity is not feasible. In convective flows the direction of heat flux is not normal to the temperature contours. In these scenarios, the heat lines provide a practical methodology for visualizing the intensity of thermal energy heat transfer and this in turn clarifies to the engineer possible channels for thermal energy transfer to occur from hot to cold walls. Kimura and Bejan [29] & Bejan [30] originated the heat line concept. For unsteady problems, Aggarwal and Manhapra [31] studied the heat lines. Similarly, Rani and Reddy [32] employed the heat lines for couple stress flows from a slender cylinder. Also, Rani et al. [33] studied the solutal version of this regime and presented detailed mass line visualizations. By using similar idea, recently Das and Basak [34] examined the rate of heat transport at different zones within the enclosures. Recently, the concept of heat line visualization for natural convection in a cavity can be found in [35,36]. More recently, Bondareva et al. [37,38] studied the heat line concept for free convection with nanofluid in open cavity. Use of heat lines approach for convection problem is revealed in [39]. Till date, little attention is devoted in the reported literature for the heat lines and first time, an attempt is made to visualize the shear thickening/shear thinning phenomenon flow behavior using this heat function concept.

Based on the literature survey, it can be observed that very scant attention has been paid to the flow over a vertical cylinder with third-grade fluid. Thus, it is focused to analyze the time-dependent third-grade fluid flow over a uniformly heated cylinder in the boundary layer region. A temperature at the wall is taken to be greater than that of surrounding fluid temperature. The transitory effects of the third-grade fluid flow are studied for the flow and heat transport coefficients for various controlling parameters and compared with the usual Newtonian fluid flow. The results obtained by the implicit finite difference method are corroborated by the available existing results in the literature.

This research article is arranged in the following ways: Sectio n "Mathematical modeling" deals with the physical model of a third-grade fluid flow over a semi-infinite vertical cylinder with uniform temperature and its non-dimensionalization. The next section dealt with the grid generation and the FDM procedure to solve the complex flow-field PDE's. In the Section "Results and discussion", the transient 2D flow-field profiles, wall and heat transfer coefficients are analyzed. Further, comparison between third-grade and Newtonian fluids are explained. Finally, in Section "Concluding remarks" the important observations are made.

## Mathematical modeling

Transient 2D laminar buoyancy driven flow of a third-grade fluid over a cylinder of radius $r_0$ is considered. The flow geometry along with specified variables is shown in Fig. 1. The rectangular coordinate system is chosen, in which the axial coordinate ($x$-axis) is selected from the foremost verge of the cylinder, while the radial coordinate ($r$-axis) is assessed normal to the $x$-axis. The neighboring fluid temperature is considered to be stationary and similar to that of free stream temperature $T'_\infty$. At $t' = 0$, the temperature $T'_\infty$ is uniform for the cylinder and surrounding environment fluid. Later ($t' > 0$), the temperature of the vertical cylinder is augmented to $T'_w (> T'_\infty)$ and preserved uniformly there afterward.

*Governing equations:*

The third-grade fluid has the following constituent equations [10,40]

$$\tau = -PI + \mu S_1 + \alpha_1^* S_2 + \alpha_2^* S_1^2 + \beta_1^* S_3 + \beta_2^* (S_1 S_2 + S_2 S_1) + \beta_3^* (tr S_1^2) S_1 \tag{1}$$

where $\tau$ is a Cauchy stress tensor, $P$ is pressure, $I$ is an identity tensor, $\alpha_i^* (i = 1, 2)$ and $\beta_i^* (i = 1, 2, 3)$ are the rheological material moduli which are temperature-dependent functions in general. It is noted that from Eq. (1), the coefficients $\beta_i^* (i = 1, 2, 3)$ are zero for the second-grade fluid, and for the classical Navier-Stokes fluid; both $\alpha_i^* (i = 1, 2)$ and $\beta_i^* (i = 1, 2, 3)$ are zero. Rivlin and Ericksen tensors $S_i (i = 1, 2, 3)$ are mentioned as follows:

$$S_1 = \nabla \mathrm{V} + (\nabla \mathrm{V})^{T^*}$$

$$S_i = \frac{dS_{i-1}}{dt} + S_{i-1}(\nabla \mathrm{V}) + (\nabla \mathrm{V})^{T^*} S_{i-1}, \quad i = 2, 3 \ldots . \tag{2}$$

where $\nabla$ is gradient operator, $T^*$ is matrix transposition, V is velocity field, $\frac{d}{dt}$ is the material time derivative defined as

$$\frac{d}{dt}(\cdot) = \left(\frac{\partial}{\partial t} + \mathrm{V}.\nabla\right)(\cdot)$$

Thermodynamic compatibility of third-grade fluid has been shown by Fosdick and Rajagopal [41]. Considering the assumption that the Helmholtz free energy is minimum at equilibrium and Clausius-Duhem inequality gives the following constraints.

$$\mu \geqslant 0, \quad \alpha_1^* \geqslant 0, \quad |\alpha_1^* + \alpha_2^*| \leqslant \sqrt{24 \mu \beta_3^*}, \quad \beta_1^* = 0, \quad \beta_2^* = 0, \quad \beta_3^* \geqslant 0$$

Substituting the above inequalities in Eq. (1), gives the following equation

$$\tau = -PI + \mu S_1 + \alpha_1^* S_2 + \alpha_2^* S_1^2 + \beta_3^* (tr S_1^2) S_1 \tag{3}$$

Using the above definitions and assumptions, the boundary layer equations for the flow of incompressible third-grade fluid in the absence of body couples along with Boussinesq's approximation are given by:

*Law of conservation of mass:*

$$\frac{\partial (ru)}{\partial x} + \frac{\partial (rv)}{\partial r} = 0 \tag{4}$$

*Law of conservation of momentum:*

$$\rho \frac{Dv}{Dt'} = -\frac{\partial P}{\partial r} + \frac{\partial \tau_{rr}}{\partial r} + \frac{\tau_{rr}}{r} + \frac{\partial \tau_{rx}}{\partial x}$$

$$\rho \frac{Du}{Dt'} = -\frac{\partial P}{\partial x} + \frac{\partial \tau_{xr}}{\partial r} + \frac{\tau_{xr}}{r} + \frac{\partial \tau_{xx}}{\partial x}$$

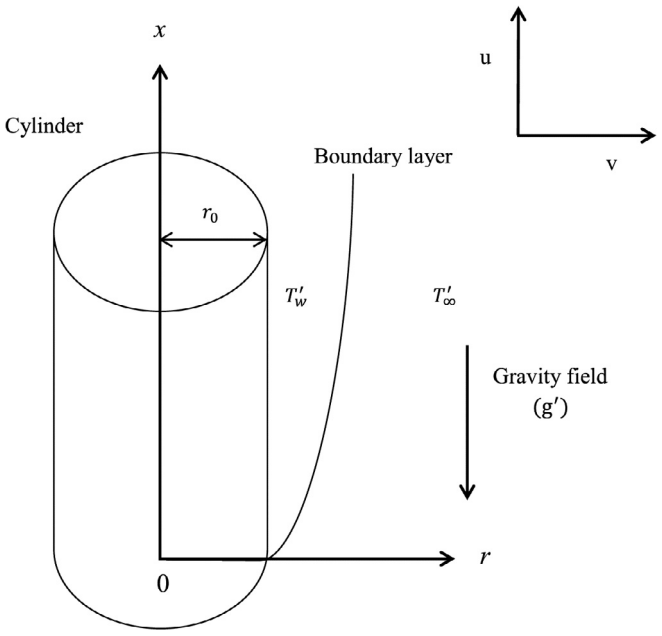


**Fig. 1.** Schematic of the investigated problem and coordinate system.

in which

$$\begin{aligned}
\tau_{rx} = \tau_{xr} = {} & \mu\left(\frac{\partial u}{\partial r} + \frac{\partial v}{\partial x}\right) + \alpha_1^*\left[\frac{\partial^2 u}{\partial r \partial t'} + \frac{\partial^2 v}{\partial x \partial t'} + v\frac{\partial^2 u}{\partial r^2} + v\frac{\partial^2 v}{\partial r \partial x}\right. \\
& + u\frac{\partial^2 v}{\partial x^2} + u\frac{\partial^2 u}{\partial x \partial r} + 3\frac{\partial u}{\partial x}\frac{\partial u}{\partial r} + 3\frac{\partial v}{\partial x}\frac{\partial v}{\partial r} + \frac{\partial u}{\partial r}\frac{\partial v}{\partial r} + \frac{\partial u}{\partial x}\frac{\partial v}{\partial x} \\
& \left. + \left(\frac{1}{r}\frac{\partial u}{\partial \theta} + \frac{\partial w}{\partial x}\right)\frac{\partial w}{\partial r} + \left(\frac{1}{r}\frac{\partial v}{\partial \theta} - \frac{w}{r} + \frac{\partial w}{\partial r}\right)\frac{\partial w}{\partial x}\right] \\
& + \alpha_2^*\left[2\frac{\partial u}{\partial r}\frac{\partial v}{\partial r} + 2\frac{\partial u}{\partial x}\frac{\partial u}{\partial r} + 2\frac{\partial v}{\partial x}\frac{\partial v}{\partial r} + 2\frac{\partial u}{\partial x}\frac{\partial v}{\partial x}\right. \\
& \left. + \left(\frac{1}{r}\frac{\partial u}{\partial \theta} + \frac{\partial w}{\partial x}\right)\left(\frac{1}{r}\frac{\partial v}{\partial \theta} - \frac{w}{r} + \frac{\partial w}{\partial r}\right)\right] \\
& + \beta_3^*\left[4\left(\frac{\partial v}{\partial r}\right)^2\left(\frac{\partial u}{\partial r} + \frac{\partial v}{\partial x}\right) + 2\left(\frac{\partial u}{\partial r} + \frac{\partial v}{\partial x}\right)^3\right. \\
& \left. + 4\left(\frac{\partial u}{\partial x}\right)^2\left(\frac{\partial u}{\partial r} + \frac{\partial v}{\partial x}\right)\right]
\end{aligned}$$

$$\begin{aligned}
\tau_{rr} = {} & 2\mu\left(\frac{\partial v}{\partial r}\right) + \alpha_1^*\left\{2\frac{\partial^2 v}{\partial r \partial t'} + 2v\frac{\partial^2 v}{\partial r^2} + 2u\frac{\partial^2 v}{\partial x \partial r}\right. \\
& \left. + 2\left[2\left(\frac{\partial v}{\partial r}\right)^2 + \frac{\partial u}{\partial r}\frac{\partial v}{\partial x} + \left(\frac{\partial u}{\partial r}\right)^2 + \left(\frac{1}{r}\frac{\partial v}{\partial \theta} - \frac{w}{r} + \frac{\partial w}{\partial r}\right)\frac{\partial w}{\partial r}\right]\right\} \\
& + \alpha_2^*\left\{4\left(\frac{\partial v}{\partial r}\right)^2 + \left(\frac{\partial v}{\partial x} + \frac{\partial u}{\partial r}\right)^2 + \left(\frac{1}{r}\frac{\partial v}{\partial \theta} - \frac{w}{r} + \frac{\partial w}{\partial r}\right)^2\right\} \\
& + \beta_3^*\left\{2\frac{\partial v}{\partial x}\left[4\left(\frac{\partial v}{\partial r}\right)^2 + 2\left(\frac{\partial u}{\partial r} + \frac{\partial v}{\partial x}\right)^2 + 4\left(\frac{\partial u}{\partial x}\right)^2\right]\right\}
\end{aligned}$$

$$\begin{aligned}
\tau_{xx} = {} & 2\mu\left(\frac{\partial u}{\partial x}\right) + \alpha_1^*\left\{2\frac{\partial^2 u}{\partial x \partial t'} + 2u\frac{\partial^2 u}{\partial x^2} + 2v\frac{\partial^2 u}{\partial x \partial r}\right. \\
& \left. + 2\left[2\left(\frac{\partial u}{\partial x}\right)^2 + \frac{\partial u}{\partial r}\frac{\partial v}{\partial x} + \left(\frac{\partial v}{\partial x}\right)^2 + \left(\frac{1}{r}\frac{\partial u}{\partial \theta} + \frac{\partial w}{\partial x}\right)\frac{\partial w}{\partial x}\right]\right\} \\
& + \alpha_2^*\left\{4\left(\frac{\partial u}{\partial x}\right)^2 + \left(\frac{\partial v}{\partial x} + \frac{\partial u}{\partial r}\right)^2 + \left(\frac{1}{r}\frac{\partial u}{\partial \theta} + \frac{\partial w}{\partial x}\right)^2\right\} \\
& + \beta_3^*\left\{2\frac{\partial u}{\partial x}\left[4\left(\frac{\partial v}{\partial r}\right)^2 + 2\left(\frac{\partial u}{\partial r} + \frac{\partial v}{\partial x}\right)^2 + 4\left(\frac{\partial u}{\partial x}\right)^2\right]\right\}
\end{aligned}$$

where $u$ and $v$ denote the velocity components along the axial ($x$) and radial ($r$) directions, respectively, $\rho$ is the density and $\tau_{rr}$, $\tau_{rx}$, $\tau_{xr}$, $\tau_{xx}$ are the extra stress components. The flow is assumed to be along the $x$-direction only and hence by neglecting along the radial direction, the momentum and energy equations are given by [26,42,43]

$$\rho\left(\frac{\partial u}{\partial t'}+u\frac{\partial u}{\partial x}+v\frac{\partial u}{\partial r}\right)=\rho g'\beta_T(T'-T'_\infty)+\frac{\mu}{r}\frac{\partial}{\partial r}\left(r\frac{\partial u}{\partial r}\right)+\alpha_1^*\left[\frac{\partial^3 u}{\partial r^2\partial t'}+\frac{1}{r}\frac{\partial^2 u}{\partial r\partial t'}+v\frac{\partial^3 u}{\partial r^3}+2\frac{\partial v}{\partial r}\frac{\partial^2 u}{\partial r^2}+3\frac{\partial^2 u}{\partial r^2}\frac{\partial u}{\partial x}+\frac{\partial u}{\partial r}\frac{\partial^2 v}{\partial r^2}+4\frac{\partial u}{\partial r}\frac{\partial^2 u}{\partial x\partial r}+\frac{v}{r}\frac{\partial^2 u}{\partial r^2}+\frac{u}{r}\frac{\partial^2 u}{\partial x\partial r}+\frac{3}{r}\frac{\partial u}{\partial x}\frac{\partial u}{\partial r}+u\frac{\partial^3 u}{\partial x\partial r^2}+\frac{1}{r}\frac{\partial u}{\partial r}\frac{\partial v}{\partial r}\right]+\alpha_2^*\left[\frac{2}{r}\frac{\partial u}{\partial r}\frac{\partial v}{\partial r}+\frac{2}{r}\frac{\partial u}{\partial x}\frac{\partial u}{\partial r}+2\frac{\partial^2 u}{\partial r^2}\frac{\partial u}{\partial x}+2\frac{\partial^2 v}{\partial r^2}\frac{\partial u}{\partial r}+2\frac{\partial v}{\partial r}\frac{\partial^2 u}{\partial r^2}+4\frac{\partial u}{\partial r}\frac{\partial^2 u}{\partial x\partial r}\right]+\beta_3^*\left[\frac{2}{r}\left(\frac{\partial u}{\partial r}\right)^3+6\left(\frac{\partial u}{\partial r}\right)^2\frac{\partial^2 u}{\partial r^2}+4\left(\frac{\partial u}{\partial r}\right)^2\frac{\partial^2 u}{\partial x^2}+2\frac{\partial u}{\partial x}\frac{\partial u}{\partial r}\frac{\partial^2 u}{\partial x\partial r}\right] \tag{5}$$

*Law of conservation of energy:*

$$\frac{\partial T'}{\partial t'}+u\frac{\partial T'}{\partial x}+v\frac{\partial T'}{\partial r}=\frac{\alpha}{r}\frac{\partial}{\partial r}\left(r\frac{\partial T'}{\partial r}\right) \tag{6}$$

The appropriate initial and boundary conditions are as follows:

$$\begin{aligned} &t'\leqslant 0: T'=T'_\infty,\ v=0,\ u=0 \quad \text{for all } x \text{ and } r\\ &t'>0: T'=T'_w,\ v=0,\ u=0 \quad \text{at } r=r_0\\ &\qquad T'=T'_\infty,\ v=0,\ u=0 \quad \text{at } x=0\\ &\qquad T'\to T'_\infty,\ v\to 0,\ u\to 0,\ \frac{\partial u}{\partial r}\to 0 \quad \text{as } r\to\infty \end{aligned} \tag{7}$$

Initiating the subsequent non-dimensional quantities

$$X=Gr^{-1}\frac{x}{r_0},\quad R=\frac{r}{r_0},\quad U=\frac{Gr^{-1}ur_0}{\vartheta},\quad V=\frac{vr_0}{\vartheta},\quad t=\frac{\vartheta t'}{r_0^2},\quad T=\frac{T'-T'_\infty}{T'_w-T'_\infty},\quad Gr=\frac{g'\beta_T r_0^3(T'_w-T'_\infty)}{\vartheta^2},\quad Pr=\frac{\vartheta}{\alpha},\quad \alpha_1=\frac{\alpha_1^*}{\rho r_0^2},\quad \alpha_2=\frac{\alpha_2^*}{\rho r_0^2},\quad \beta=\frac{\beta_3^*\vartheta}{\rho r_0^4} \tag{8}$$

(for the above symbols refer nomenclature) in the Eqs. (4)–(6) and also in Eq. (7), they reduce to subsequent form

$$\frac{\partial U}{\partial X}+\frac{\partial V}{\partial R}+\frac{V}{R}=0 \tag{9}$$

**Table 1**
Grid independence test for selecting mesh size.

| Grid size | Average Nusselt number $\overline{Nu}$ for $Pr$ = 0.63 and $\alpha_1=\alpha_2=\beta=0.2$. |
|---|---|
| 25 × 125 | .754702700000000000000000 |
| 50 × 250 | .748941600000000000000000 |
| 100 × 500 | .747439000000000000000000 |
| 200 × 1000 | .747371100000000000000000 |

$$\frac{\partial U}{\partial t}+U\frac{\partial U}{\partial X}+V\frac{\partial U}{\partial R}=T+\frac{1}{R}\frac{\partial}{\partial R}\left(R\frac{\partial U}{\partial R}\right)+\alpha_1\left[\frac{\partial^3 U}{\partial R^2\partial t}+\frac{1}{R}\frac{\partial^2 U}{\partial R\partial t}+V\frac{\partial^3 U}{\partial R^3}+2\frac{\partial V}{\partial R}\frac{\partial^2 U}{\partial R^2}+3\frac{\partial^2 U}{\partial R^2}\frac{\partial U}{\partial X}+\frac{\partial U}{\partial R}\frac{\partial^2 V}{\partial R^2}+4\frac{\partial U}{\partial R}\frac{\partial^2 U}{\partial X\partial R}+\frac{V}{R}\frac{\partial^2 U}{\partial R^2}+\frac{U}{R}\frac{\partial^2 U}{\partial X\partial R}+\frac{3}{R}\frac{\partial U}{\partial X}\frac{\partial U}{\partial R}+U\frac{\partial^3 U}{\partial X\partial R^2}+\frac{1}{R}\frac{\partial U}{\partial R}\frac{\partial V}{\partial R}\right]+\alpha_2\left[\frac{2}{R}\frac{\partial U}{\partial R}\frac{\partial V}{\partial R}+\frac{2}{R}\frac{\partial U}{\partial X}\frac{\partial U}{\partial R}+2\frac{\partial^2 U}{\partial R^2}\frac{\partial U}{\partial X}+2\frac{\partial^2 V}{\partial R^2}\frac{\partial U}{\partial R}+2\frac{\partial V}{\partial R}\frac{\partial^2 U}{\partial R^2}+4\frac{\partial U}{\partial R}\frac{\partial^2 U}{\partial X\partial R}\right]+\beta\left[(Gr)^2\frac{2}{R}\left(\frac{\partial U}{\partial R}\right)^3+6(Gr)^2\left(\frac{\partial U}{\partial R}\right)^2\frac{\partial^2 U}{\partial R^2}+4\left(\frac{\partial U}{\partial R}\right)^2\frac{\partial^2 U}{\partial X^2}+2\frac{\partial U}{\partial X}\frac{\partial U}{\partial R}\frac{\partial^2 U}{\partial X\partial R}\right] \tag{10}$$

$$\frac{\partial T}{\partial t}+U\frac{\partial T}{\partial X}+V\frac{\partial T}{\partial R}=\frac{1}{Pr}\left(\frac{\partial^2 T}{\partial R^2}+\frac{1}{R}\frac{\partial T}{\partial R}\right) \tag{11}$$

$$\begin{aligned} &t\leqslant 0: T=0,\ V=0,\ U=0 \quad \text{for all } X \text{ and } R\\ &t>0: T=1,\ V=0,\ U=0 \quad \text{at } R=1\\ &\qquad T=0,\ V=0,\ U=0 \quad \text{at } X=0\\ &\qquad T\to 0,\ V\to 0,\ U\to 0,\ \frac{\partial U}{\partial R}\to 0 \quad \text{as } R\to\infty \end{aligned} \tag{12}$$

**Table 2**
Grid independence test for selecting time step size.

| Time step size ($\Delta t$) | Average Nusselt number $\overline{Nu}$ for $Pr$ = 0.63 and $\alpha_1=\alpha_2=\beta=0.2$. |
|---|---|
| 0.1 | .747709900000000000000000 |
| 0.08 | .747723600000000000000000 |
| 0.05 | .747642600000000000000000 |
| 0.02 | .747564900000000000000000 |
| 0.01 | .747439000000000000000000 |

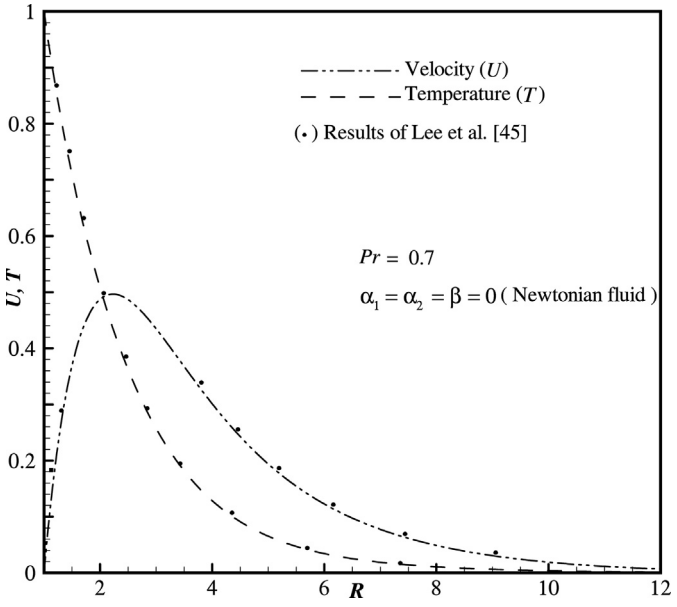


**Fig. 2.** Comparison of flow field variables.

## Finite difference solution procedure

Let $JR = \frac{1}{1+(g-1)\Delta R}$. Using Crank-Nicolson method, the finite difference equations to the above Eqs. (9)–(11) are as follows:

$$\frac{U_{f,g}^{h+1}-U_{f-1,g}^{h+1}+U_{f,g}^{h}-U_{f-1,g}^{h}}{2\Delta X}+\frac{V_{f,g}^{h+1}-V_{f,g-1}^{h+1}+V_{f,g}^{h}-V_{f,g-1}^{h}}{2\Delta R}+V_{f,g}^{h+1}(JR)=0 \tag{13}$$

$$\begin{aligned}
&\frac{U_{f,g}^{h+1}-U_{f,g}^{h}}{\Delta t}+\frac{U_{f,g}^{h}}{2\Delta X}\left(U_{f,g}^{h+1}-U_{f-1,g}^{h+1}+U_{f,g}^{h}-U_{f-1,g}^{h}\right)\\
&+\frac{V_{f,g}^{h}}{4\Delta R}\left(U_{f,g+1}^{h+1}-U_{f,g-1}^{h+1}+U_{f,g+1}^{h}-U_{f,g-1}^{h}\right)\\
&=\frac{T_{f,g}^{h+1}+T_{f,g}^{h}}{2}+\frac{JR}{4\Delta R}\left(U_{f,g+1}^{h+1}-U_{f,g-1}^{h+1}+U_{f,g+1}^{h}-U_{f,g-1}^{h}\right)\\
&+\frac{1}{2(\Delta R)^2}\left(U_{f,g-1}^{h+1}-2U_{f,g}^{h+1}+U_{f,g+1}^{h+1}+U_{f,g-1}^{h}-2U_{f,g}^{h}+U_{f,g+1}^{h}\right)\\
&+\alpha_1\left[\frac{1}{4(\Delta R)^2(\Delta t)}\left(U_{f,g-2}^{h+1}-2U_{f,g}^{h+1}+U_{f,g+2}^{h+1}-U_{f,g-2}^{h}+2U_{f,g}^{h}-U_{f,g+2}^{h}\right)\right.\\
&+\frac{JR}{2(\Delta R)(\Delta t)}\left(U_{f,g+1}^{h+1}-U_{f,g-1}^{h+1}-U_{f,g+1}^{h}+U_{f,g-1}^{h}\right)\\
&+\frac{V_{f,g}^{h}}{4(\Delta R)^3}\left(U_{f,g+2}^{h+1}-2U_{f,g+1}^{h+1}+2U_{f,g-1}^{h+1}-U_{f,g-2}^{h+1}+U_{f,g+2}^{h}\right.\\
&\left.-2U_{f,g+1}^{h}+2U_{f,g-1}^{h}-U_{f,g-2}^{h}\right)\\
&+\frac{1}{2(\Delta R)^3}\left(V_{f,g+1}^{h}-V_{f,g-1}^{h}\right)\left(U_{f,g-1}^{h+1}-2U_{f,g}^{h+1}+U_{f,g+1}^{h+1}+U_{f,g-1}^{h}\right.\\
&\left.-2U_{f,g}^{h}+U_{f,g+1}^{h}\right)+\frac{3}{2(\Delta X)(\Delta R)^2}\left(U_{f,g}^{h}-U_{f-1,g}^{h}\right)\left(U_{f,g-1}^{h+1}-2U_{f,g}^{h+1}\right.\\
&\left.+U_{f,g+1}^{h+1}+U_{f,g-1}^{h}-2U_{f,g}^{h}+U_{f,g+1}^{h}\right)\\
&+\frac{1}{4(\Delta R)^3}\left(U_{f,g+1}^{h+1}-U_{f,g-1}^{h+1}+U_{f,g+1}^{h}-U_{f,g-1}^{h}\right)\left(V_{f,g-1}^{h}\right.\\
&\left.-2V_{f,g}^{h}+V_{f,g+1}^{h}\right)+\frac{1}{2(\Delta X)(\Delta R)^2}\left(U_{f,g+1}^{h}-U_{f,g-1}^{h}\right)\left(U_{f,g+1}^{h+1}\right.\\
&\left.-U_{f-1,g+1}^{h+1}-U_{f,g-1}^{h+1}+U_{f-1,g-1}^{h+1}+U_{f,g+1}^{h}-U_{f-1,g+1}^{h}-U_{f,g-1}^{h}+U_{f-1,g-1}^{h}\right)\\
&+\frac{V_{f,g}^{h}JR}{2(\Delta R)^2}\left(U_{f,g-1}^{h+1}-2U_{f,g}^{h+1}+U_{f,g+1}^{h+1}+U_{f,g-1}^{h}-2U_{f,g}^{h}+U_{f,g+1}^{h}\right)\\
&+\frac{U_{f,g}^{h}JR}{4(\Delta R)(\Delta X)}\left(U_{f,g+1}^{h+1}-U_{f-1,g+1}^{h+1}-U_{f,g-1}^{h+1}+U_{f-1,g-1}^{h+1}+U_{f,g+1}^{h}\right.\\
&\left.-U_{f-1,g+1}^{h}-U_{f,g-1}^{h}+U_{f-1,g-1}^{h}\right)\\
&+\frac{3JR}{4(\Delta R)(\Delta X)}\left(U_{f,g}^{h}-U_{f-1,g}^{h}\right)\left(U_{f,g+1}^{h+1}-U_{f,g-1}^{h+1}+U_{f,g+1}^{h}-U_{f,g-1}^{h}\right)\\
&+\frac{U_{f,g}^{h}}{2(\Delta R)^2(\Delta X)}\left(U_{f,g+1}^{h+1}-U_{f-1,g+1}^{h+1}-2U_{f,g}^{h+1}+2U_{f-1,g}^{h+1}+U_{f,g-1}^{h+1}\right.\\
&\left.-U_{f-1,g-1}^{h+1}+U_{f,g+1}^{h}-U_{f-1,g+1}^{h}-2U_{f,g}^{h}+2U_{f-1,g}^{h}+U_{f,g-1}^{h}-U_{f-1,g-1}^{h}\right)\\
&\left.+\frac{JR}{8(\Delta R)^3}\left(V_{f,g+1}^{h}-V_{f,g-1}^{h}\right)\left(U_{f,g+1}^{h+1}-U_{f,g-1}^{h+1}+U_{f,g+1}^{h}-U_{f,g-1}^{h}\right)\right]\\
&+\alpha_2\left[\frac{JR}{4(\Delta R)^2}\left(V_{f,g+1}^{h}-V_{f,g-1}^{h}\right)\left(U_{f,g+1}^{h+1}-U_{f,g-1}^{h+1}+U_{f,g+1}^{h}-U_{f,g-1}^{h}\right)\right.\\
&+\frac{JR}{2(\Delta R)(\Delta X)}\left(U_{f,g}^{h}-U_{f-1,g}^{h}\right)\left(U_{f,g+1}^{h+1}-U_{f,g-1}^{h+1}+U_{f,g+1}^{h}-U_{f,g-1}^{h}\right)\\
&+\frac{1}{(\Delta X)(\Delta R)^2}\left(U_{f,g}^{h}-U_{f-1,g}^{h}\right)\left(U_{f,g-1}^{h+1}-2U_{f,g}^{h+1}+U_{f,g+1}^{h+1}+U_{f,g-1}^{h}\right.\\
&\left.-2U_{f,g}^{h}+U_{f,g+1}^{h}\right)+\frac{1}{2(\Delta R)^3}\left(V_{f,g-1}^{h}-2V_{f,g}^{h}+V_{f,g+1}^{h}\right)\left(U_{f,g+1}^{h+1}\right.\\
&\left.-U_{f,g-1}^{h+1}+U_{f,g+1}^{h}-U_{f,g-1}^{h}\right)\\
&+\frac{1}{2(\Delta X)(\Delta R)^2}\left(U_{f,g+1}^{h}-U_{f,g-1}^{h}\right)\left(U_{f,g+1}^{h+1}-U_{f-1,g+1}^{h+1}-U_{f,g-1}^{h+1}\right.\\
&\left.+U_{f-1,g-1}^{h+1}+U_{f,g+1}^{h}-U_{f-1,g+1}^{h}-U_{f,g-1}^{h}+U_{f-1,g-1}^{h}\right)\\
&+\frac{1}{2(\Delta R)^3}\left(V_{f,g+1}^{h}-V_{f,g-1}^{h}\right)\left(U_{f,g-1}^{h+1}-2U_{f,g}^{h+1}\right.\\
&\left.\left.+U_{f,g+1}^{h+1}+U_{f,g-1}^{h}-2U_{f,g}^{h}+U_{f,g+1}^{h}\right)\right]\\
&+\beta\left[\frac{JR(Gr)^2}{4(\Delta R)^3}\left(U_{f,g+1}^{h}-U_{f,g-1}^{h}\right)^3\right.\\
&+\frac{3(Gr)^2}{4(\Delta R)^4}\left(U_{f,g+1}^{h}-U_{f,g-1}^{h}\right)^2\left(U_{f,g-1}^{h+1}-2U_{f,g}^{h+1}+U_{f,g+1}^{h+1}\right.\\
&\left.+U_{f,g-1}^{h}-2U_{f,g}^{h}+U_{f,g+1}^{h}\right)\\
&+\frac{1}{(\Delta X)^2(\Delta R)^2}\left(U_{f-1,g}^{h}-2U_{f,g}^{h}+U_{f+1,g}^{h}\right)\left(U_{f,g+1}^{h}-U_{f,g-1}^{h}\right)^2\\
&+\frac{1}{8(\Delta X)^2(\Delta R)^2}\left(U_{f,g}^{h}-U_{f-1,g}^{h}\right)\left(U_{f,g+1}^{h}-U_{f,g-1}^{h}\right)\left(U_{f,g+1}^{h+1}\right.\\
&-U_{f-1,g+1}^{h+1}-U_{f,g-1}^{h+1}+U_{f-1,g-1}^{h+1}+U_{f,g+1}^{h}\\
&\left.\left.-U_{f-1,g+1}^{h}-U_{f,g-1}^{h}+U_{f-1,g-1}^{h}\right)\right]
\end{aligned} \tag{14}$$

$$\begin{aligned}
&\frac{T_{f,g}^{h+1}-T_{f,g}^{h}}{\Delta t}+\frac{U_{f,g}^{h}}{2\Delta X}\left(T_{f,g}^{h+1}-T_{f-1,g}^{h+1}+T_{f,g}^{h}-T_{f-1,g}^{h}\right)\\
&+\frac{V_{f,g}^{h}}{4\Delta R}\left(T_{f,g+1}^{h+1}-T_{f,g-1}^{h+1}+T_{f,g+1}^{h}-T_{f,g-1}^{h}\right)\\
&=\frac{1}{2Pr(\Delta R)^2}\left(T_{f,g-1}^{h+1}-2T_{f,g}^{h+1}+T_{f,g+1}^{h+1}+T_{f,g-1}^{h}-2T_{f,g}^{h}+T_{f,g+1}^{h}\right)\\
&+\frac{JR}{4Pr\Delta R}\left(T_{f,g+1}^{h+1}-T_{f,g-1}^{h+1}+T_{f,g+1}^{h}-T_{f,g-1}^{h}\right)
\end{aligned} \tag{15}$$

The results of these equations obtained in the rectangular grid with $X_{min}=0$, $X_{max}=1$, $R_{min}=1$ and $R_{max}=20$ where $R_{max}$ relates to $R=\infty$ which lies far away from the boundary layer. Eqs. (15), (14) at the $(h+1)$th stage is specified in the following tri-diagonal and penta-diagonal forms:

$$A_1\varphi_{f,g-1}^{h+1}+B_1\varphi_{f,g}^{h+1}+C_1\varphi_{f,g+1}^{h+1}=D_1$$

$$A_2\omega_{f,g-2}^{h+1}+B_2\omega_{f,g-1}^{h+1}+C_2\omega_{f,g}^{h+1}+D_2\omega_{f,g+1}^{h+1}+E_2\omega_{f,g+2}^{h+1}=F_2$$

where $\varphi$ and $\omega$ indicates the time-dependent flow-field variables $T$ and $U$. Thus, Eqs. (15) and (14) at each interior grid point on a precise $f$-level comprise a system of tri-diagonal and penta-diagonal equations. For more detailed description of this finite difference scheme can be found in the available literature Rani et al. [44].

*Validation of the numerical scheme using grid independent test:*

A grid independent test has been conducted for different grid sizes and the values of the average Nusselt number $\overline{Nu}$ for the control parameters $Pr=0.63$, $\alpha_1=\alpha_2=\beta=0.2$ on the boundary $R=1$ is shown in Table 1. It is noticed from Table 1 a uniform grid size of $100\times500$ is enough for this study. Similarly, a time-independence test has been performed for different time step sizes, as shown in Table 2. The effective selected time step size $\Delta t$ $(t=h\Delta t, h=0,1,2,\ldots)$ is fixed as 0.01.

## Results and discussion

The computer-generated flow-field variables in the case of Newtonian fluids $(\alpha_1=\alpha_2=\beta=0)$ are similar to those of Lee et al. [45] for Prandtl number $(Pr)=0.7$ and are illustrated in

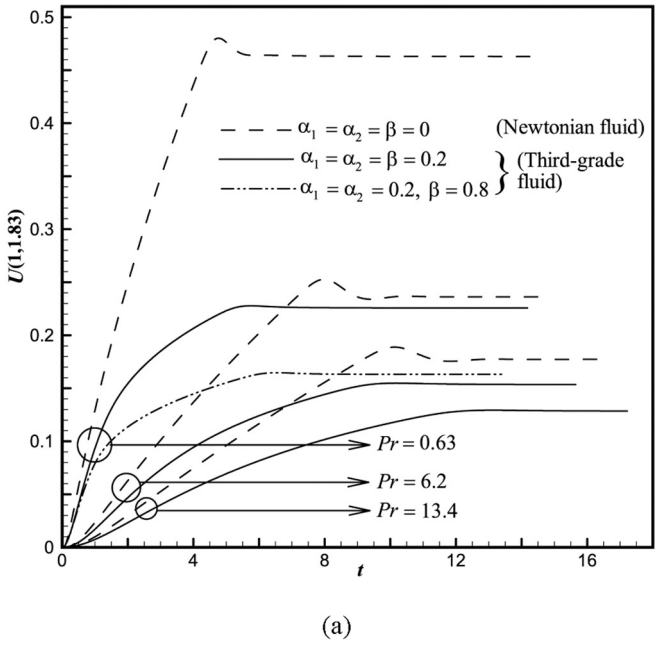


**Fig. 3.** Time-dependent velocity profile ($U$) versus time ($t$) for various values of control parameters at the location (a) (1, 1.83); (b) (1, 5.82).

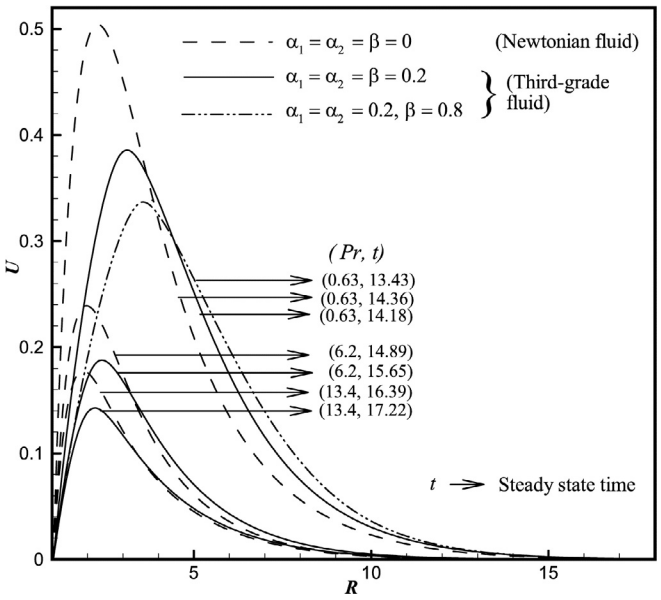


**Fig. 4.** Simulated time-independent state velocity profile ($U$) versus $R$ at $X$ = 1.0 for various values of control parameters.

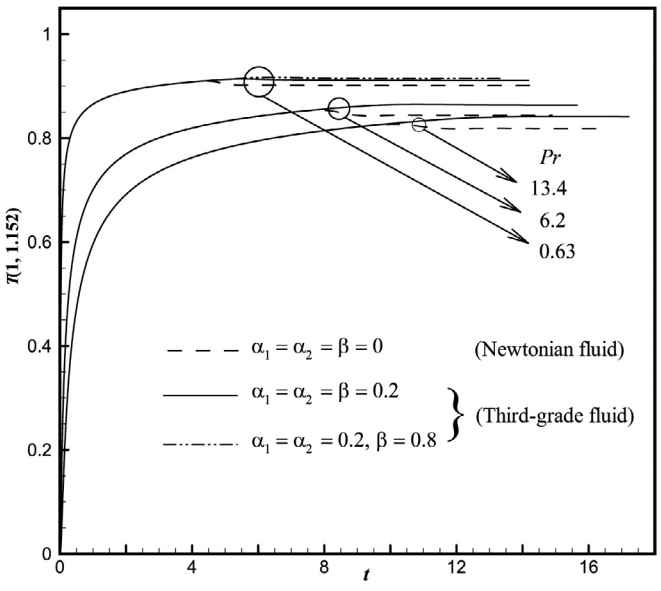


**Fig. 5.** Simulated time-dependent temperature profile ($T$) versus time $t$ for different values of control parameters at the location (1, 1.152).

Fig. 2. The outcomes are found to be in good covenant. The influence of the control parameters, namely, *Pr* [=0.63 (oxygen), 6.2 (dichlorodifluoromethane), 13.4 (sea water at 0 °C)], second-grade fluid parameters $\alpha_1, \alpha_2$ [=0, 0.2] and third-grade fluid parameter $\beta$ [=0, 0.2, 0.8] on the flow field are analyzed. The selected chemical compounds for the present investigated problem using *Pr* is an obvious choice because of its widespread usage in many industrial applications. For example, dichlorodifluoromethane is used as a coolant in refrigerators, air conditioners and in automobiles, etc. because of its interesting properties such as non-corrosive to mechanical components, non-toxic, non-flammable, low boiling point and high heat of vaporization. Similarly, the other compounds also have many applications.

*Flow variables*

The simulated velocity ($U$) against time ($t$) at (1, 1.83) and (1, 5.82) locations for different control parameters is graphically shown in Fig. 3. The $U$ profiles, in Fig. 3a and b, are taken in the vicinity and far away from the hot cylindrical wall, respectively. At all positions, the velocity curves augment with time, attains the temporal maxima then become independent of time. For instance, $\alpha_1 = \alpha_2 = \beta = 0.2$ and *Pr* = 0.63, with time the wall velocity monotonically escalates, reaches temporal maxima and in the end, reaches the time-independent state. Also, it is perceived that when $t << 1$, the conduction dominates the convection. Then the heat transport coefficient is swayed by the convection effect due

to escalated upward velocities. From Fig. 3a, it is noticed that the velocities get overshoot before attaining the steady-state. Here, the overshoot of the $U$ profile diminishes as $Pr$ gets augmented. The incentive behind this decrement is that increasing $Pr$ values amplifies the size of velocity diffusion term in Eq. (10), and thus, there is a lesser amount of resistance to the flow of fluid in the province of the temporal maxima of velocity. Also, the time to attain the temporal maxima increases for rising values of $Pr$. The transient characteristics of temperature shown in Fig. 5 are similar to those of velocity profile and will be discussed later. From Fig. 3a it is observed that for all values of $Pr$ the transient velocity values of the third-grade fluid ($\beta > 0$) are less than that of the Newtonian fluid ($\alpha_1 = \alpha_2 = \beta = 0$). While the opposite tendency observed in Fig. 3b.

Fig. 4 elucidates the steady-state non-dimensional $U$ profile for different control parameters. Here, it is perceived that the $U$ curves begin with the no-slip boundary condition, reaches its peak value and then shrinkages to zero along the radial position ($R$) satisfying the far-away boundary conditions. The effect of $\beta$ and $Pr$ on velocity profile is revealed in this figure. The time to attain the steady-state rises with augmenting values of $Pr$ or decreasing $\beta$. Since the influence of velocity diffusion gets amplified for higher $Pr$ values, and hence the velocity gets minimized. The $U$ profile for the third-grade fluid gets more deviated from the hot cylindrical wall compared to that of a Newtonian fluid. Also, adjacent to the hot cylindrical wall the velocity regarding its magnitude is high for the Newtonian fluids and is less for the third-grade fluids, while this trend gets reversed far away from the thermal boundary. For example, fixing $Pr = 0.63$, it is noticed that the velocity profile of the third-grade fluid is less than those of the Newtonian fluid in the region, $1 < R < 3.7$ while the opposite trend is observed for $R > 3.7$. Hence there is a significant difference between the transient velocity profiles of the third-grade fluid and the Newtonian fluid.

Simulated transient temperature ($T$) profile is drawn at $(1, 1.152)$ with time in Fig. 5. Initially, these patterns increase with time and later they become independent of time. This transient behavior of the temperature is observed at other locations also. For enlarged $Pr$, initially, the profiles of the third-grade fluid and Newtonian fluid have concurred with each other. For instance, when $Pr = 6.2$, $\alpha_1 = \alpha_2 = \beta = 0.2$, the temperature profile of a third-grade fluid gets deviated from the Newtonian fluid, which is approximately at $t = 7.6$. For all values of $Pr$, the $T$ profile for third-grade fluids ($\beta > 0$) is higher than usual Newtonian fluids ($\alpha_1 = \alpha_2 = \beta = 0$).

The temperature profile ($T$) against $R$ at steady-state about $Pr$ and $\beta$ is shown in Fig. 6. These patterns begin with the boundary value of $T = 1$ and then reduce to zero. This is because of the velocity diffusion effect that gets amplified with $Pr$ and higher velocity is observed in the neighborhood of the hot cylindrical wall. Also, for amplifying $Pr$ or decreasing $\beta$, the time needed to attain time-independent state for temperature profile gets augmented. Also, with increasing $Pr$, the $T$ profile for third-grade fluid is larger than that of a Newtonian fluid. The critical observation in this figure is, as $\beta$ increases, the thermal boundary layer becomes thicker. This case is reversed with higher $Pr$, since a higher $Pr$ means, instead

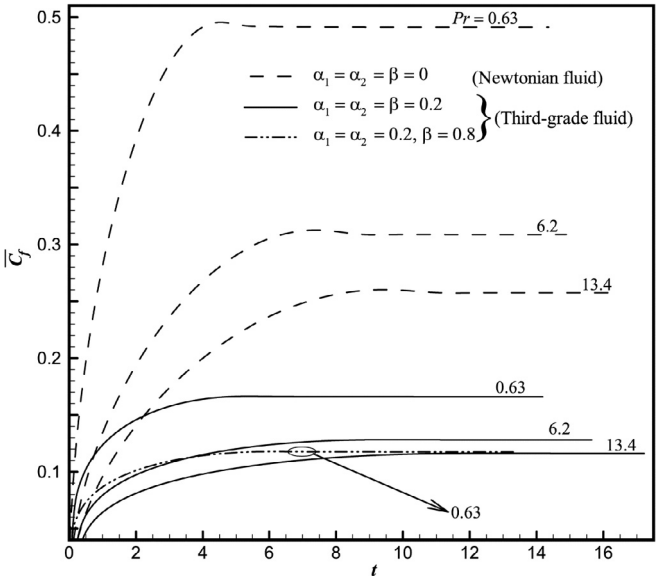


**Fig. 7.** Average momentum transport coefficient ($\overline{C_f}$) for various values of control parameters.

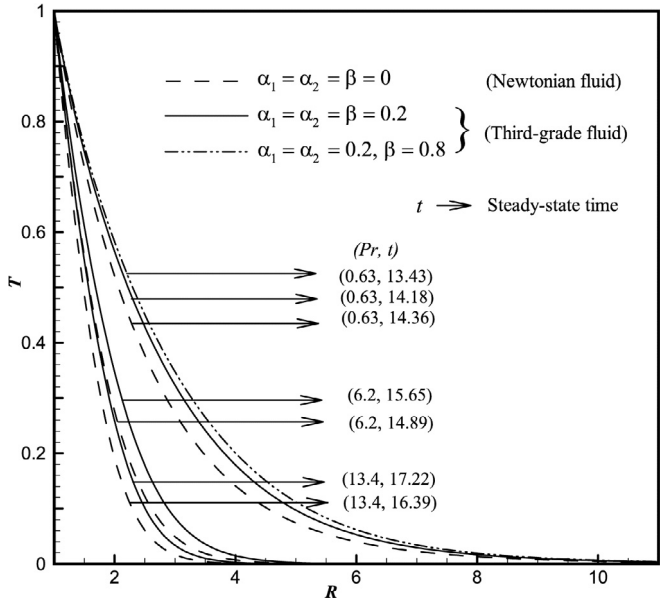


**Fig. 6.** Simulated time-independent state temperature profile ($T$) versus $R$ at $X = 1.0$ for various values of control parameters.

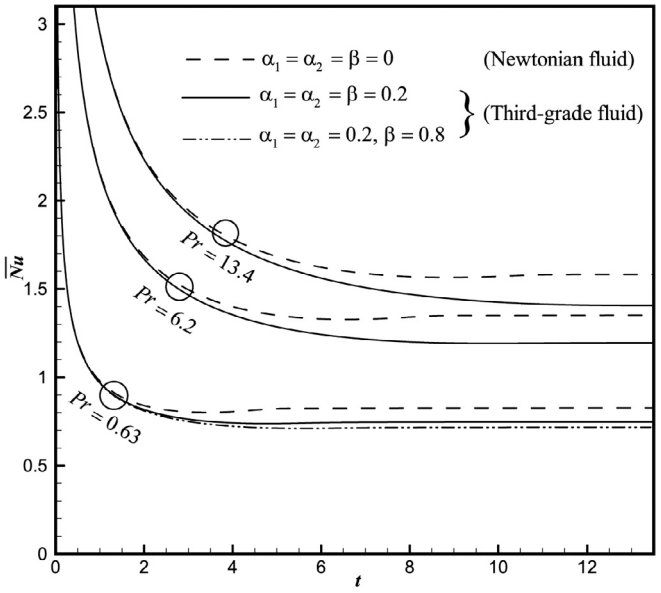


**Fig. 8.** Average heat transport coefficient ($\overline{Nu}$) for various values of control parameters.

of thermal diffusion the velocity diffusion tries to diverge from the hot wall. Also for increasing *Pr*, the deviation of the steady-state *T* curves from the hot cylindrical wall is observed. This variation increases for a third-grade fluid than the Newtonian fluid. Hence, in this section, it is remarked that the *T* profiles for the third-grade fluid vary significantly with a Newtonian fluid.

*Friction and heat transport coefficients*

Thermal flow-field transport coefficients for the non-Newtonian third-grade fluid are significant parameters in the convection heat transfer studies. The average friction and heat transport coefficients in non-dimensional form are given by

$$\overline{C_f} = \int_0^1 \left(\frac{\partial U}{\partial R}\right)_{R=1} dX \quad \text{and} \quad \overline{Nu} = -\int_0^1 \left(\frac{\partial T}{\partial R}\right)_{R=1} dX \text{ respectively.}$$

The values of $\overline{C_f}$ against time ($t$) for different control parameters are presented in Fig. 7. It is noted from this figure, for all *Pr* and β values the $\overline{C_f}$ oscillate initially and at last becomes asymptotically steady. Also, for increasing values of *Pr* or β, the $\overline{C_f}$ decreases. In particular, as *Pr* upsurges, the $\overline{C_f}$ of a third-grade fluid is not as much of the Newtonian fluid.

The $\overline{Nu}$ for several values of *Pr* and β are revealed in Fig. 8. It is perceived that the $\overline{Nu}$ upsurges with *Pr*. Also, for each *Pr* value, the $\overline{Nu}$ decreases for third-grade fluid and amplifies for a Newtonian fluid. Amplifying *Pr*, accelerates the spatial decay of the temperature field close to the heated surface, yielding an upsurge in the heat transport coefficient. Also, for a particular *Pr*, the $\overline{Nu}$ decreases with augmenting values of β.

*Stream and heat functions*

The fluid motion is simulated using the non-dimensional stream function ψ, which satisfies the Eq. (9). The relationship between ψ, *U* and *V* for 2D flows is given as:

$$U = \frac{1}{R}\frac{\partial \psi}{\partial R} \quad \& \quad V = -\frac{1}{R}\frac{\partial \psi}{\partial X} \tag{16}$$

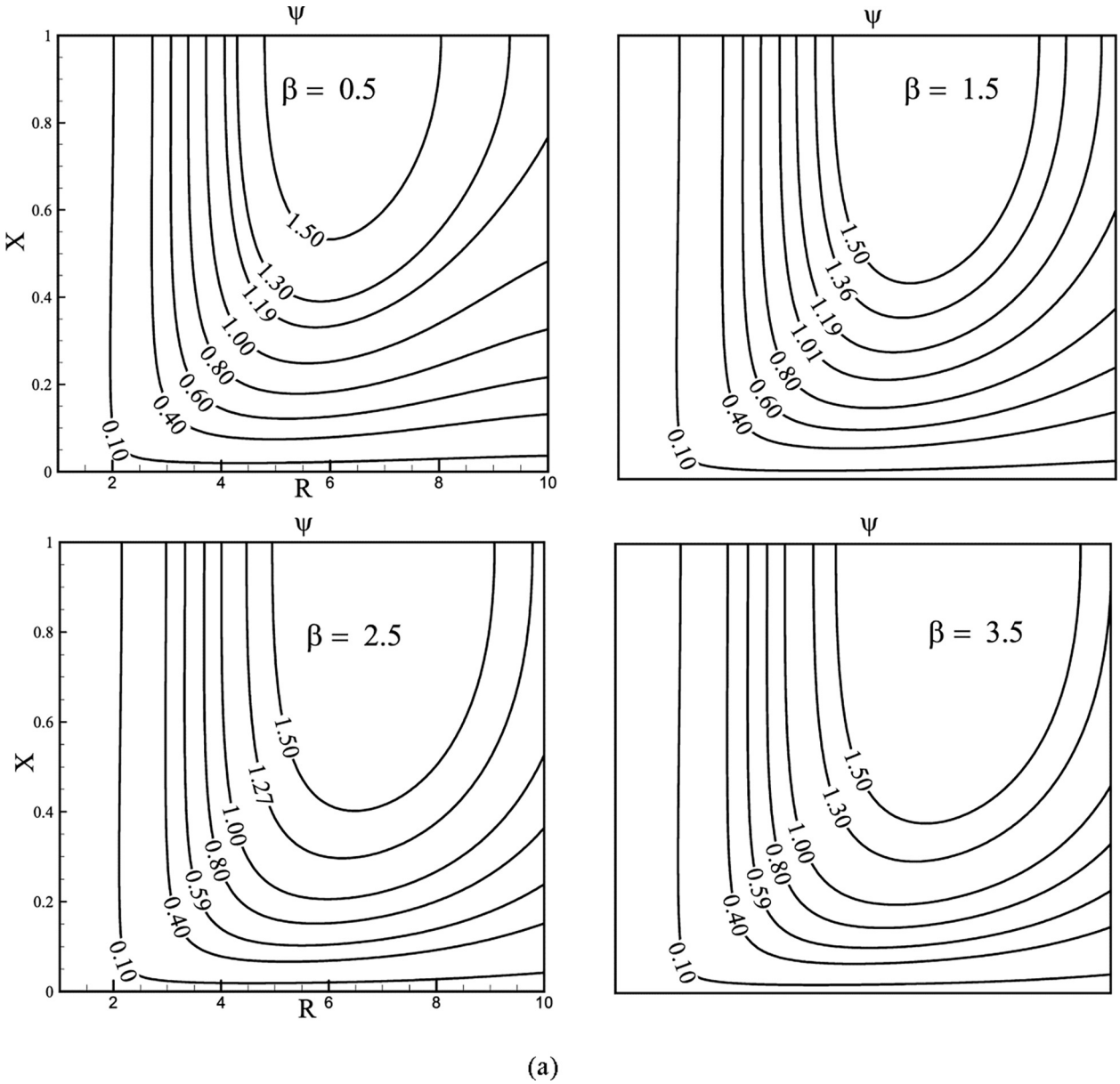


**Fig. 9.** Time-independent state (a) streamlines (ψ); (b) isotherms (*T*) and (c) heat lines (Ω) for various values of β with fixed values of $\alpha_1 = \alpha_2 = 0.2$ and *Pr* = 0.63.

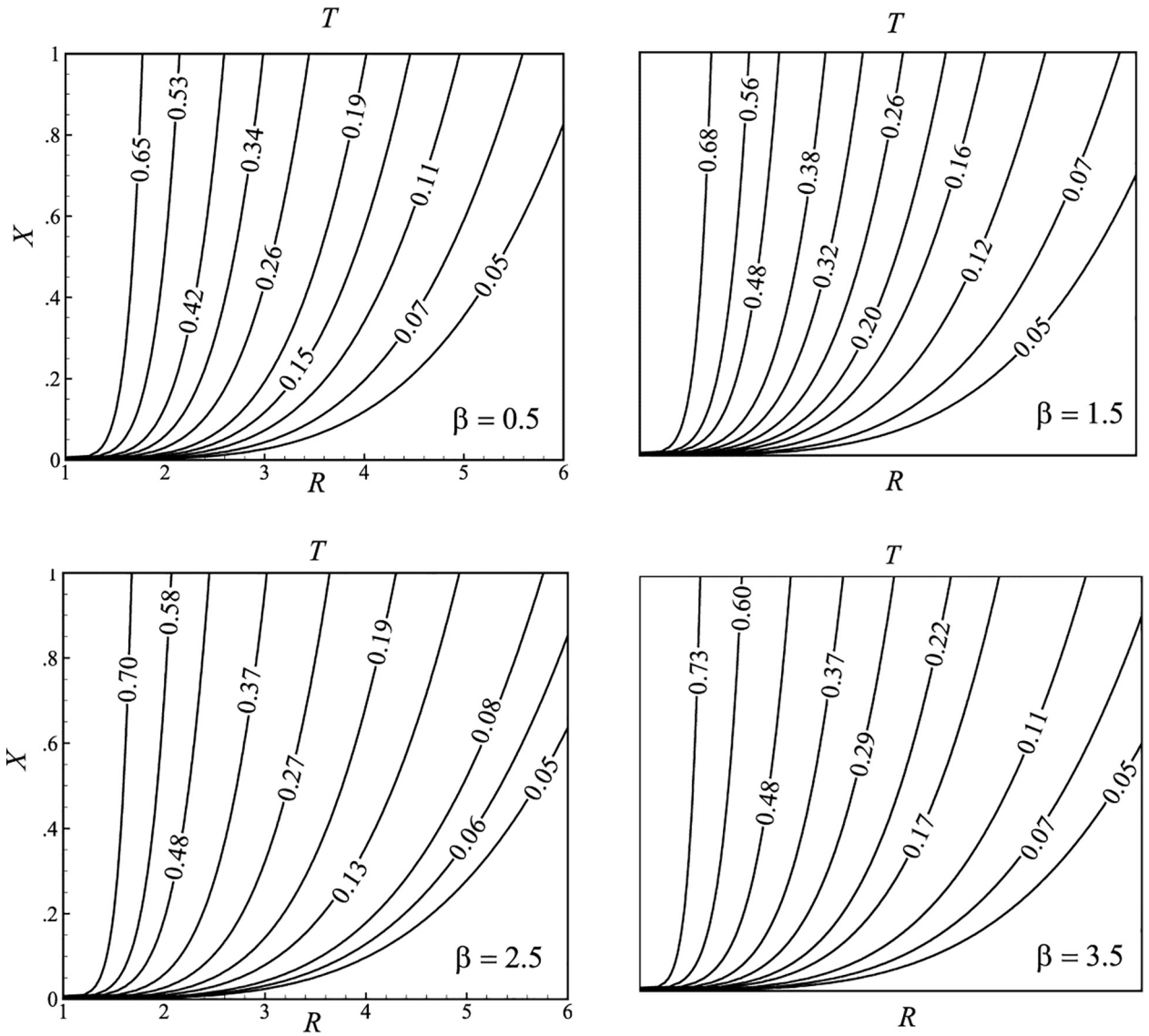


(b)

**Fig. 9** (*continued*)

This equation yields

$$\frac{\partial^2\psi}{\partial X^2}+\frac{\partial^2\psi}{\partial R^2}=U+R\frac{\partial U}{\partial R}-R\frac{\partial V}{\partial X} \tag{17}$$

Similarly, the heat function $\Omega'$ for the temperature distribution is defined as

$$\frac{\partial\Omega'}{\partial x}=\rho r v C_p(T'-T'_\infty)-kr\frac{\partial T'}{\partial r} \tag{18a}$$

$$-\frac{1}{r}\frac{\partial\Omega'}{\partial r}=\rho u C_p(T'-T'_\infty) \tag{18b}$$

Clearly $\Omega'$ satisfies the steady-state thermal energy Eq. (6). The non-dimensional heat function $\Omega=\frac{\Omega'}{k(T'_w-T'_\infty)r_0Gr}$, renders the heat function dimensionless. It can be noted that the maximum value of this function equals the overall average $\overline{Nu}$ on the hot wall.

Eqs. (18a) and (18b) in terms of $\Omega$ can be re-written as

$$\frac{\partial\Omega}{\partial X}=Pr(RVT)-R\frac{\partial T}{\partial R} \tag{19a}$$

$$-\frac{\partial\Omega}{\partial R}=Pr(RUT) \tag{19b}$$

Also, the above equations identically satisfy the thermal equation Eq. (11) in time-independent state form. Using Eqs. (19a) and (19b), one can obtain the following heat function equation (Poisson equation) as

$$\frac{\partial^2\Omega}{\partial X^2}+\frac{\partial^2\Omega}{\partial R^2}=Pr\left[\frac{\partial(VT)}{\partial X}-R\frac{\partial(UT)}{\partial R}-UT\right]-R\frac{\partial^2 T}{\partial X\partial R} \tag{20}$$

The values of $\psi$ and $\Omega$, are calculated using the central finite differences of second-order. The steady-state streamlines, isotherms, and heat lines are represented in Fig. 9 for different values of β. It can be viewed that the variation in heat lines occurs in the proximity of the hot cylindrical wall compared to usual streamlines and

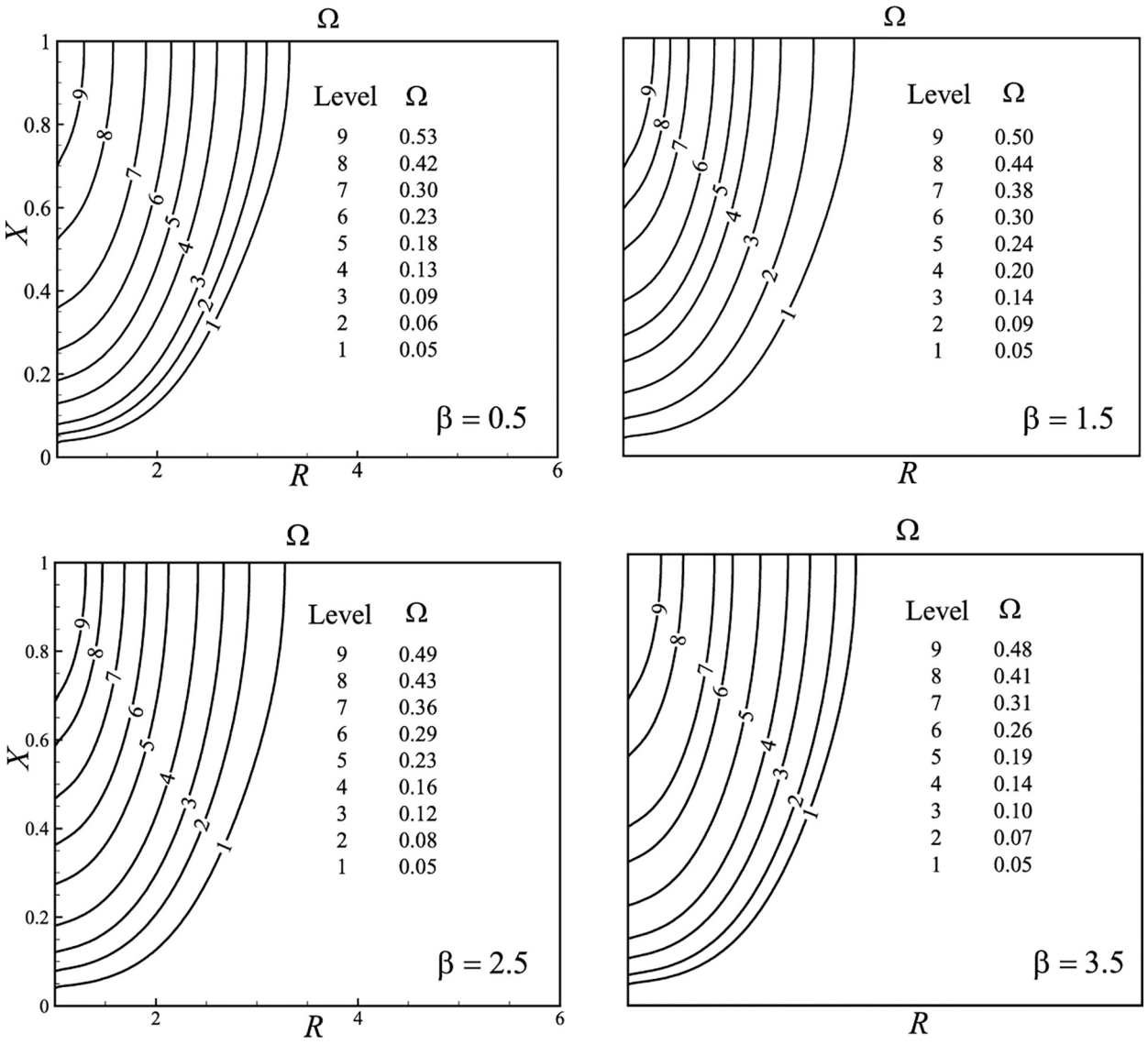


(c)

**Fig. 9** (*continued*)

isotherms. From Fig. 9a, it is seen that the heat transfer strength from the wall to the third-grade fluid is maximum for cumulative values of $X$, and it declines as $X$ decreases. The heat lines shown in Fig. 9c perceived to have a similar propensity to that of isotherms as shown in Fig. 9b. However, to understand the flow visualization and heat transfer mechanism the heat lines are the best tool as compared to isotherms. Also, as β augments, the maximum value of Ω decreases, since the $\overline{Nu}$ decreases on the hot wall. It is further noticed that these heat lines move towards far away from the heated wall for lower values of β, but the reverse trend is seen in the case of isotherms.

*Comparison between third-grade and Newtonian fluid flows*

Fig. 10 elucidates the $U$ and $T$ contours for third-grade and Newtonian fluid flows with the fixed $Pr = 0.63$. The velocity of the third-grade fluid (i.e., Fig. 10b) flow is noticed to be smaller than the usual Newtonian fluid (i.e., Fig. 10a) flow, whereas for the $T$ distribution the reverse trend is observed. Also, the $T$ contours for the third-grade fluid are to some extent different, with bigger temperature layer, as compared to Newtonian fluid.

## Concluding remarks

Flow visualization is explored using Bejan's heat line concept to investigate the time-dependent free convective third-grade fluid flow past a cylinder. The Crank-Nicolson technique has been applied to solve the normalized, partial differential conservation equations for momentum and energy conservation. The physical characteristics of heat lines are immensely beneficial in visualizing heat transfer in the 2D domain. Also in a given rectangular computational domain, the heat lines provide a powerful method for evaluating the heat transfer rate at all levels. The simulations are carried out for different non-dimensional numbers Prandtl number ($Pr$), second-grade fluid parameters ($\alpha_1, \alpha_2$) and third-grade fluid parameter (β). The time needed for the flow profiles to attain the

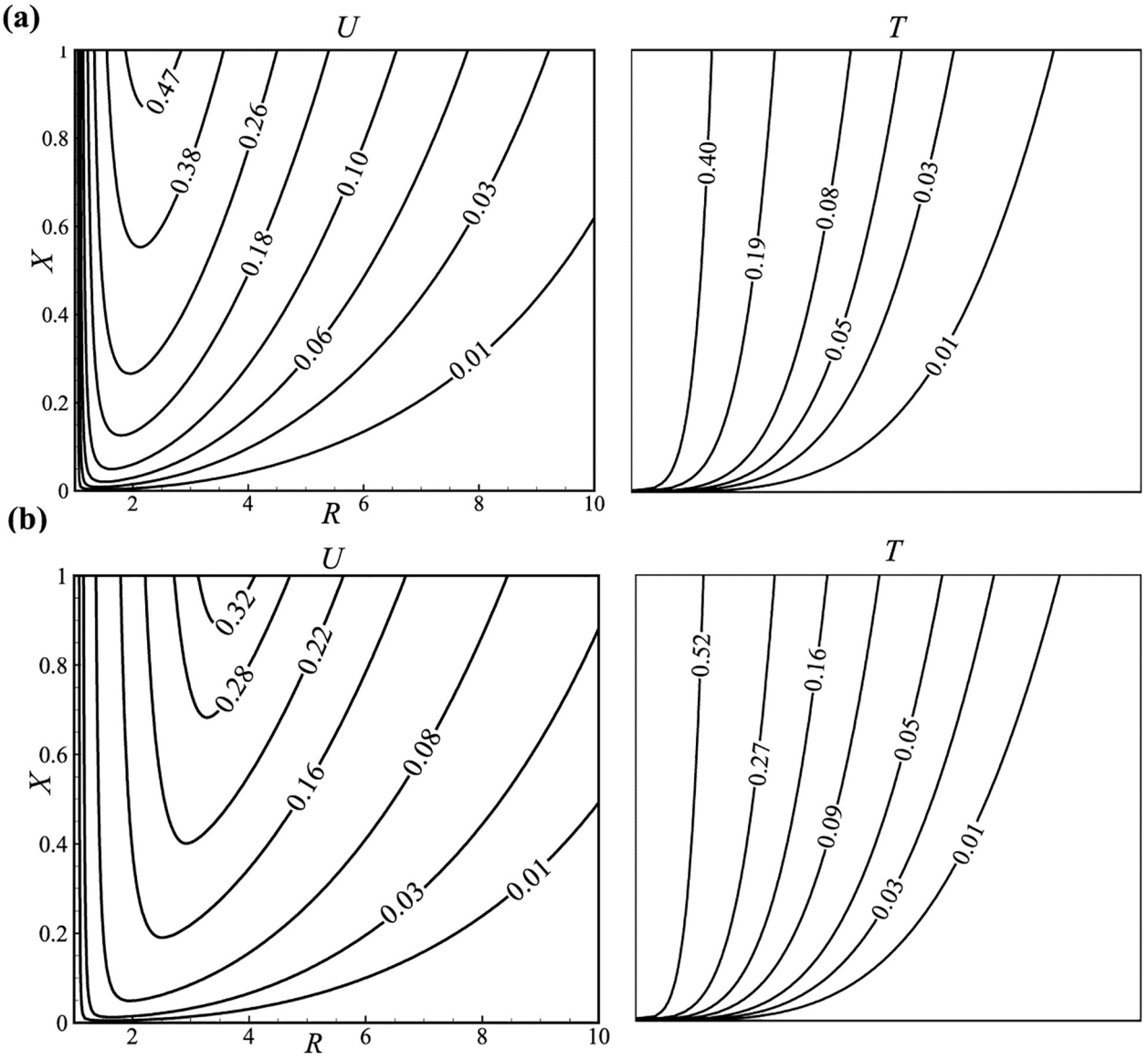


**Fig. 10.** Time-independent state contours of velocity ($U$) and temperature ($T$) with fixed value of $Pr = 0.63$ for (a) Newtonian fluid ($\alpha_1 = \alpha_2 = \beta = 0$); (b) Third-grade fluid ($\alpha_1 = \alpha_2 = \beta = 0.2$).

steady-state amplifies with increasing values of $Pr$ or decreasing values of $\beta$. The wall shear stress and heat transport coefficients at the heated wall decrease as $\beta$ increases. It is noticed that as $\beta$ decreases, the deviations of heat function contours from the hot cylindrical wall increases. Also, as $\beta$ increases, the maximum value of $\Omega$ decreases. Flow visualization indicates that the streamlines occur in the entire two-dimensional domain, while the isotherms and heat lines exist in a finite region, which is observed adjacent to the hot cylindrical wall only. Finally, from this study, it can be concluded that the flow profiles in both transient and steady-state condition, average heat and momentum transport coefficients of the third-grade fluid ($\beta > 0$) flow vary considerably from those of the Newtonian fluid ($\alpha_1 = \alpha_2 = \beta = 0$).

## Acknowledgements

The second author Ashwini Hiremath and third author Mahesh Kumar wishes to thank DST-INSPIRE (Code No.'s: IF160409, IF160028) for the grant of research fellowships and to Central University of Karnataka for providing the research facilities.

## References

[1] Guha A, Pradhan K. Natural convection of non-Newtonian power-law fluids on a horizontal plate. Int J Heat Mass Transfer 2014;70:930–8.
[2] Khandelwal V, Dhiman A, Baranyi L. Laminar flow of non-Newtonian shear-thinning fluids in a T-channel. Comput Fluids 2015;108:79–91.
[3] Miroshnichenko IV, Sheremet MA, Pop I. Natural convection in a trapezoidal cavity filled with a micropolar fluid under the effect of a local heat source. Int J Mech Sci 2017;120:182–9.
[4] Khalil UrR, Khan AA, Malik MY, Zehra I, Ali U. Temperature and concentration stratification effects on non-Newtonian fluid flow past a cylindrical surface. Results Phys 2017;7:3659–67.
[5] Rani HP, Reddy GJ. Soret and Dufour effects on transient double diffusive free convection of couple-stress fluid past a vertical cylinder. J Appl Fluid Mech 2013;6:545–54.
[6] Odelu O, Adigoppula R, Pravin KK. Influence of thermophoresis and induced magnetic field on chemically reacting mixed convective flow of Jeffrey fluid between porous parallel plates. J Mol Liq 2017;232:195–206.
[7] Pop I. Free convection in a square cavity filled with a Casson fluid under the effects of thermal radiation and viscous dissipation. Int J Numer Methods Heat Fluid Flow 2017;27:238–2332.
[8] Umavathi JC, Sheremet MA. Onset of double-diffusive convection of a sparsely packed micropolar fluid in a porous medium layer saturated with a nanofluid. Microfluid Nanofluid 2017;21:1–22.
[9] Rivlin RS, Ericksen JL. Stress deformation relations for isotropic materials. J Ration Mech Anal 1955;4:323–425.

[10] Truesdell C, Noll W. The non-linear field theories of mechanics. In: Handbuch. Physik, Vol. III/3. New York: Springer; 1965.
[11] Schowalter WR. Mechanics of non-Newtonian fluids. Oxford: Pergamon Press; 1978.
[12] Huilgol RR. Continuum mechanics of viscoelastic liquids. Delhi: Hindustan Publishing Corporation; 1975.
[13] Rajagopal KR, Gupta AS. On a class of exact solutions to the equations of motion of a second grade fluid. Int J Eng Sci 1981;19:1009–14.
[14] Rajagopal KR, Gupta AS. An exact solution for the flow of a non-Newtonian fluid past an infinite porous plate. Meccanica 1984;19:158–60.
[15] Rajagopal KR, Kaloni PN. Some remarks on the boundary conditions for fluids of differential type. In: Graham GAC, Malik SK, editors. Continuum mechanics and its applications. New York: Hemisphere; 1989. p. 935–42.
[16] Dunn JE, Rajagopal KR. Fluids of differential type: critical review and thermodynamic analysis. Int J Eng Sci 1995;33:689–729.
[17] Rajagopal KR, Szeri AZ, Troy W. An existence theorem for the flow of non-Newtonian fluid past an infinite porous plate. Int J Non-linear Mech 1986;21:279–89.
[18] Abbasbandy S, Hayat T. On series solution for unsteady boundary layer equations in a special third grade fluid. Commun Nonlinear Sci Numer Simul 2011;16:3140–6.
[19] Hayat T, Shafiq A, Alsaedi A, Awais M. MHD axisymmetric flow of third grade fluid between stretching sheets with heat transfer. Comput Fluids 2013;86:103–8.
[20] Massoudi M, Christie I. Effects of variable viscosity and viscous dissipation on the flow of third grade fluid in pipe. Int J Non-linear Mech 1995;30:687–99.
[21] Pakdemirli M. The boundary layer equations of third-grade fluids. Int J Non-linear Mech 1992;27:785–93.
[22] Hayat T, Awais M, Asghar S, Obaidat S. Unsteady flow of third grade fluid with Soret and Dufour effects. ASME J Heat Transfer 2012;134. 062001–7.
[23] Hayat T, Shafiq A, Alsaedi A. MHD axisymmetric flow of third grade fluid by a stretching cylinder. Alex Eng J 2015;54:205–12.
[24] Samuel OA, Oluwole DM. Thermodynamic analysis for a third-grade fluid through a vertical channel with internal heat generation. J Hydrodynamics, Ser B 2015;27:264–72.
[25] Samuel OA, Falade JA. Thermodynamics analysis of hydromagnetic third grade fluid flow through a channel filled with porous medium. Alex Eng J 2015;54:615–22.
[26] Hayat T, Nazar H, Imtiaz M, Alsaedi A, Ayub M. Axisymmetric squeezing flow of third grade fluid in presence of convective conditions. Chin J Phys 2017;55:738–54.
[27] Imtiaz M, Alsaedi A, Shafiq A, Hayat T. Impact of chemical reaction on third grade fluid flow with Cattaneo-Christov heat flux. J Mol Liq 2017;229:501–7.
[28] Samuel OA, Falade JA, Jangili S, Beg OA. Irreversibility analysis for reactive third-grade fluid flow and heat transfer with convective wall cooling. Alex Eng J 2017;56:153–60.
[29] Kimura S, Bejan A. The heatline visualization of convective heat transfer. ASME J Heat Transfer 1983;105:916–9.
[30] Bejan A. Convection heat transfer. 1st ed. New York: John Wiley and Sons; 1984.
[31] Aggarwal SK, Manhapra A. Use of heatlines for unsteady buoyancy-driven flow in a cylindrical enclosure. ASME J Heat Transfer 1989;111:576–8.
[32] Rani HP, Reddy GJ. Heatline visualization for conjugate heat transfer of a couple stress fluid from a vertical slender hollow cylinder. Int Commun Heat Mass Transfer 2013;48:46–52.
[33] Rani HP, Reddy GJ, Kim CN, Rameshwar Y. Transient couple stress fluid past a vertical cylinder with Bejan's heat and mass flow visualization for steady-state. ASME J Heat Transfer 2015;137:32501–12.
[34] Das D, Basak T. Analysis of average Nusselt numbers at various zones for heat flow visualizations during natural convection within enclosures (square vs triangular) involving discrete heaters. Int Commun Heat Mass Transfer 2016;75:303–10.
[35] Alsabery AI, Chamkha AJ, Saleh H, Hashim I. Heatline visualization of conjugate natural convection in a square cavity filled with nanofluid with sinusoidal temperature variations on both horizontal walls. Int J Heat Mass Transfer 2016;100:835–50.
[36] Hussein AK, Hussain SH. Heatline visualization of natural convection heat transfer in an inclined wavy cavities filled with nanofluids and subjected to a discrete isoflux heating from its left sidewall. Alex Eng J 2016;55:169–86.
[37] Bondareva NS, Sheremet MA, Oztop HF, Abu-Hamdeh N. Heatline visualization of MHD natural convection in an inclined wavy open porous cavity filled with a nanofluid with a local heater. Int J Heat Mass Transfer 2016;99:872–81.
[38] Bondareva NS, Sheremet MA, Oztop HF, Abu-Hamdeh N. Heatline visualization of natural convection in a thick walled open cavity filled with a nanofluid. Int J Heat Mass Transfer 2017;109:175–86.
[39] Morega A. The heat function approach to the thermomagnetic convection of electroconductive melts. Revue roumaine des Sciences Techniques. Electrotechnique et energetique 1988;33:359–68.
[40] Bikash S. Flow and heat transfer of an electrically conducting third grade fluid past an infinite plate with partial slip. Meccanica 2010;45:319–30.
[41] Fosdick RL, Rajagopal KR. Thermodynamics and stability of fluids of third grade. Proc R Soc London. Ser A 1980;369:351–77.
[42] Hayat T, Mustafa M, Asghar S. Unsteady flow with heat and mass transfer of a third grade fluid over a stretching surface in the presence of chemical reaction. Nonlinear Anal: Real World Appl 2010;11:3186–97.
[43] Sajid M, Hayat T, Asghar S. Non-similar solution for the axisymmetric flow of a third-grade fluid over a radially stretching sheet. Acta Mech 2007;189:193–205.
[44] Rani HP, Reddy GJ, Kim CN. Transient analysis of diffusive chemical reactive species for couple stress fluid flow over vertical cylinder. Appl Math Mech 2013;34:985–1000.
[45] Lee HR, Chen TS, Armaly BF. Natural convection along slender vertical cylinders with variable surface temperature. ASME J Heat Transfer 1988;110:103–8.